JGR Earth Surface

RESEARCH ARTICLE
10.1029/2023JF007574

Four Years of Meander-Bend Evolution Captured by Drone-Based Lidar Reveals Lack of Width Maintenance on the White River, Indiana, USA

H. K. Martin[1,2,3], **D. A. Edmonds**[1], **and Q. W. Lewis**[4]

[1]Department of Earth & Atmospheric Sciences, Indiana University, Bloomington, IN, USA, [2]Division of Geological and Planetary Sciences, California Institute of Technology, Pasadena, CA, USA, [3]Resnick Sustainability Institute, California Institute of Technology, Pasadena, CA, USA, [4]Department of Geography and Environmental Management, University of Waterloo, Waterloo, ON, Canada

Key Points:

- We collected 22 drone-based lidar scans of a single, rapidly migrating point bar and cutbank over 4.5 years
- We observed high spatial and temporal variability in both point bar and cutbank deposition and erosion
- The point bar did not accrete enough to match cutbank erosion, continuing an apparent ~55 years of overall meander-bend widening

Supporting Information:

Supporting Information may be found in the online version of this article.

Correspondence to:

H. K. Martin,
hkm@caltech.edu

Citation:

Martin, H. K., Edmonds, D. A., & Lewis, Q. W. (2024). Four years of meander-bend evolution captured by drone-based lidar reveals lack of width maintenance on the White River, Indiana, USA. *Journal of Geophysical Research: Earth Surface*, *129*, e2023JF007574. https://doi.org/10.1029/2023JF007574

Received 1 DEC 2023
Accepted 7 MAY 2024

Author Contributions:

Conceptualization: H. K. Martin, D. A. Edmonds, Q. W. Lewis
Data curation: H. K. Martin, Q. W. Lewis
Formal analysis: H. K. Martin, D. A. Edmonds
Funding acquisition: D. A. Edmonds
Investigation: H. K. Martin
Methodology: H. K. Martin, D. A. Edmonds, Q. W. Lewis
Resources: D. A. Edmonds
Supervision: D. A. Edmonds
Visualization: H. K. Martin
Writing – original draft: H. K. Martin
Writing – review & editing: H. K. Martin, D. A. Edmonds, Q. W. Lewis

Abstract Meandering rivers experience fluctuations in width whenever riverbanks migrate in different directions or at different rates, which can be observed after individual floods. However, meandering rivers maintain approximately constant widths over decadal timescales. This implies some timescale below which width fluctuates as banks migrate independently, and above which width is maintained by a bank-coupling process. This coupling is thought to occur either as point bar deposition events induce cutbank erosion (bar-push), or as cutbank erosion events induce point bar deposition (bank-pull). This coupling, however, has been challenging to observe in natural rivers due to limited event-scale field data. We present results from a 4.5-year campaign with 22 drone-based lidar surveys of a single point bar and cutbank (~0.35 km^2 in area) on the White River near Worthington, Indiana, USA. The middle point bar experienced net erosion (5,400 m^3), but net aggradation (17,100 m^3) between 2019 and 2022 when including perennially submerged regions. This aggradation was less than the 35,700 m^3 of cutbank erosion over the same period. Combined, we have observed widening (1.58 m/yr bend-averaged; 3.08 m/yr near apex) over the study period as point bar deposition has not kept up with cutbank erosion. Finally, we suggest that the difference between bar-push and bank-pull as width-maintenance mechanisms may not be resolvable by observing bend widening or narrowing alone without an advancement of current theory, such as determining a long-term equilibrium width and measuring deviations relative thereto.

Plain Language Summary Rivers are critical resources for humans, their economies, and the environment. Meandering rivers gradually wander across landscapes as their inner banks grow and their outer banks erode. Our understanding of this growth and erosion is still limited over the timespan of individual floods, which are likely the events that cause river movement. Partly due to a lack of observations, this is a critical knowledge gap that needs to be filled for humans to more-safely build and live alongside rivers. Over 4.5 years, we collected 22 high-resolution laser scans of the landscape of a single meandering river bend on the White River near Worthington, Indiana, USA. We tracked growth and erosion by comparing these maps to one another. We found complex behavior occurring due to individual floods, but that year-over-year changes are more predictable. While the research community has a long-held understanding that meandering rivers generally have stable widths over decades (unless water or sediment supplied to the river change), we used historical aerial photographs and modern laser scanning to find that this bend has been widening for >45 years.

1. Introduction

At the reach scale, meandering rivers translate laterally following channel curvature (Furbish, 1988; Sylvester et al., 2019). At the bank scale, meandering is achieved through sediment deposition on inner point bars and erosion on outer cutbanks. Despite more than 70 years of study across field sites, flumes, remote sensing data, and numerical models, it remains challenging to quantify the spatial and temporal variability of these processes and resultant morphology. Furthermore, while previous work has shown that meandering rivers maintain their widths as they evolve over decadal timescales (Lopez Dubon & Lanzoni, 2019; Mason & Mohrig, 2019; Nanson & Hickin, 1983), we lack event-scale observations and a practical understanding of the coupling process that accomplishes this maintenance in natural systems (Parker et al., 2011). It is important for river scientists and engineers to understand the mechanics of meandering because rivers constitute critical resources for sustaining environmental, economic, and societal wellbeing.

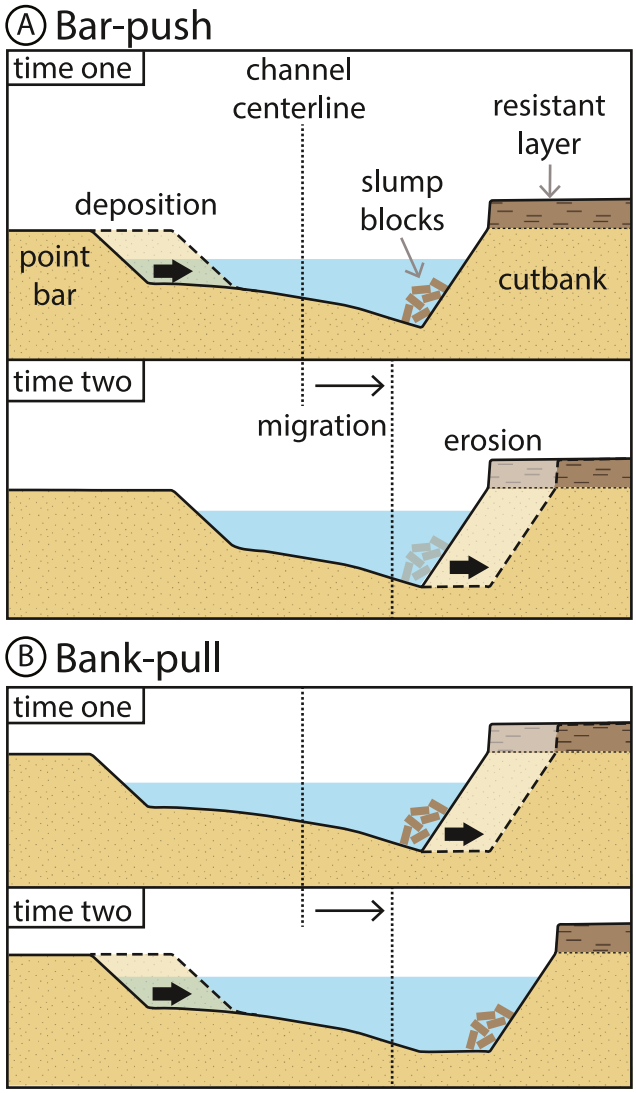

Figure 1. Two possible mechanisms to allow rivers to maintain width as they meander. Schematics show cross-section differences in the order of events between (a) bar-push (where deposition on a point bar narrows the channel to induce erosion on the cutbank) and (b) bank-pull (where erosion on a cutbank widens the channel and induces deposition on the point bar). In both cases, cutbank erosion begins with erosion of a non-cohesive lower layer, leading to cantilever failure of a resistant upper layer. Adapted from Parker et al. (2011).

Two mechanisms for such a coupling have been proposed (Figure 1). The first is called bar-push, where an initial depositional event on the point bar narrows the river and deflects flow toward the outer bank, inducing erosion. The second is called bank-pull, where an initial erosional event on the cutbank slackens flow and induces deposition on the point bar (Parker et al., 2011). While laboratory flume (van de Lageweg et al., 2014) or indirect field (Constantine et al., 2014) evidence has been used to support bar-push or bank-pull as drivers of river meandering, it has been more challenging to directly observe either of these drivers in natural settings. These sort of observations have only recently been made more accessible with the advent of repeat lidar measurements. Recent and impactful advances have come from repeat airborne lidar surveys of the coastal Trinity River (Mason & Mohrig, 2018, 2019). An initial assessment that compared two scans collected 4 years apart interpreted that, based on net deposition and faster point bar migration than cutbank migration, meandering on bends above the backwater limit is driven by bar-push. Conversely, on the basis of net deposition and faster cutbank migration than point bar migration, meandering on bends below the backwater limit was interpreted to be driven by bank-pull (Mason & Mohrig, 2018). However, upon considering a third scan collected 2 years later, nearly all bends that had narrowed between the first two scans had widened between the second two, and vice versa (Mason & Mohrig, 2019). Given the reversal of changes in channel width between scans, the authors noted that measuring or validating bar push or bank pull mechanisms in natural systems may be "extremely difficult if not impossible." Regardless, the authors provided field evidence that inner and outer riverbanks can migrate independently over event-to-annual scales but maintain an approximately constant channel width over decadal scales.

The lack of a clear understanding of bar push and bank pull has hampered understanding of meandering mechanics and subsequent model development. Early numerical models of river meandering assumed that motion on one bank would be equally matched by motion on the other (Hasegawa, 1977; Ikeda et al., 1981). However, laboratory experiments have shown that rivers developing in noncohesive unvegetated sediment will experience cutbank erosion that inevitably outpaces point bar deposition, leading to runaway channel widening (Federici & Paola, 2003). As such, these rivers will initially form meanders but transition to braided patterns before substantial sinuosity is developed (Federici & Seminara, 2003). To continually meander, riverbanks need mechanisms to enhance point bar deposition, hinder cutbank erosion, or both (Braudrick et al., 2009; Tal & Paola, 2010). While rivers can naturally meander without vegetation, particularly when muddy sediment stabilizes banks (Ielpi et al., 2022; Lapôtre et al., 2019; Smith, 1998), vegetation remains a major driver in inducing point bar deposition by reducing flow shear stress and stabilizing existing sediments (Corenblit et al., 2020; Gurnell, 2014; Hickin, 1984; Lightbody et al., 2019; Rominger et al., 2010; Yamasaki et al., 2021). Cutbank erosion can be hindered when muddy, steep-faced upper units experience cantilever failure as underlying, less-resistant unconsolidated layers are eroded (Parker et al., 2011; Stott, 1997; Thorne & Tovey, 1981), draping the exposed cutbank surface in slump blocks that shield it from further erosion until they can be destroyed or removed by future flows (Gabet, 1998; Douglas et al., 2023; Figure 1). More recently, numerical models with independently moving vegetated or cohesive banks show promise when schemes for bar-push and bank-pull are implemented heuristically; in doing so, these models predicted that meandering rivers will eventually come to an equilibrium width (Asahi et al., 2013; Eke et al., 2014; Zhao et al., 2021).

Measurements with greater temporal frequency are needed to unpack the mechanics of point bar deposition, cutbank erosion, and how rivers use bar-push or bank-pull to maintain width over decadal scales. We present the

results of a 4.5-year study in which we collected 22 drone-based lidar surveys of a single paired point bar and cutbank (~0.35 km^2 in area). Compared to typical airborne lidar, drone-based lidar offers both improved temporal resolution (due to a lower cost per survey) and improved spatial resolution. This allows us to observe changes associated with the individual floods that cause bank motion. Each survey resolves cm-scale vertical changes with sub-meter horizontal resolution. Combining these surveys with hydrologic and bathymetric observations, we study the spatial and temporal variability of bend-scale geomorphic change on a sand-bedded meandering river. There was overall minor net-erosion of the middle point bar, which was only submerged during floods, over the study period. Here, erosion and deposition were poorly predicted by flood magnitude over timescales from individual floods to multiple years. Cutbank erosion was spatially discontinuous and punctuated at the flood event scale but appeared continuous when integrated over a multi-year scale. We also found flood magnitude to be a good predictor of cutbank, but not total bend, volumetric changes. In sum, the meander bend at our study site has widened over a ~55 year period (since it formed after a cut-off sometime between 1965 and 1970), including over the study period. Finally, we suggest that the difference between bar-push and bank-pull events may not be resolvable by observing meander bend widening and narrowing on natural rivers without an advancement of current theory.

2. Field Site

The White River runs from central to southwestern Indiana, USA, with landcover varying between forests and farmed silt- and clay-rich soils (David et al., 2017). The studied bend is just downstream of a straightaway and the confluence with the smaller Eel River near Worthington, IN, USA (Figure 2a). Bend-averaged width was 144 m and maximum width was 185 m during our first scan in April 2018. The cutbank floodplain sits about 5.5 m above the channel bed, as do the inner bank scroll bars. Historic aerial photographs indicate that some time between 1965 and 1970 the river experienced a cutoff immediately upstream of our study site (dashed red box in Figure 2a; Figures S1–S5 in Supporting Information S1). These aerial photographs also indicate that the current cutbank of the meander bend has been farmed since at least 1952. A short section of cutbank is protected by riprap, and an embayment of large woody debris resulting from cutbank erosion through a stand of trees is present in the southeast (Figures 2c–2e). At the location of maximum erosion, the cutbank eroded 327 m between 1977 and 2018 (7.98 m/yr).

The Newberry, IN USGS station (03360500; USGS, 2023) is ~20 km to the south, lists a drainage area of ~12,000 km^2, and, since 1928, has recorded an average daily mean discharge between 25 m^3/s in the winter and 200 m^3/s in the spring. The hydrograph over our study period showed 44 USGS-defined "action" stage events, 19 minor floods, 2 moderate floods, and no major floods; this is fewer extreme flood events than was typical for this station over the previous 90 years (Figures 2g and 2h). Based on our measurements, the "minor floods" approximately correspond to flow at or above bankfull (Figure 2h). For validation of the Newberry station data, we installed our own water surface elevation gage in early 2020 (Figures 2c and 2e). Precipitation averaged about 1.14 m per year over the study period (NOAA NCEI, 2023), which was an increase of about 0.15 m over late 1800s hydroclimate (Widhalm et al., 2018).

3. Methods

3.1. Data Collection

A series of 22 drone-based lidar scans were collected between April 2018 and November 2022 (Figure 2h; Martin, Edmonds, & Lewis, 2024). Scans were collected before and after floods whenever possible. As the lidar sensor could not penetrate water, measurements on the lower point bar were only possible at lower water levels. For each point cloud, we removed non-ground points to create bare earth models. Drone-based lidar yielded a higher point density than is typical for airborne lidar, allowing the point clouds to be converted to raster DEMs with 0.25×0.25 m pixels. We propagated both measurement and processing errors through our workflow, yielding a minimum uncertainty of 5 cm based on uncertainties in GPS base station position and between-flightline residuals (see Supporting Information). While we were able to resolve the bare earth through the forest canopy, point densities are the greatest on flat, unvegetated surfaces, and thus uncertainty is the smallest on the subaerially exposed point bar. Short shrubs or dense tall grasses are the greatest impediment to bare-earth elevations, both because fewer bare-earth points are collected and because ground classification is more ambiguous. A full

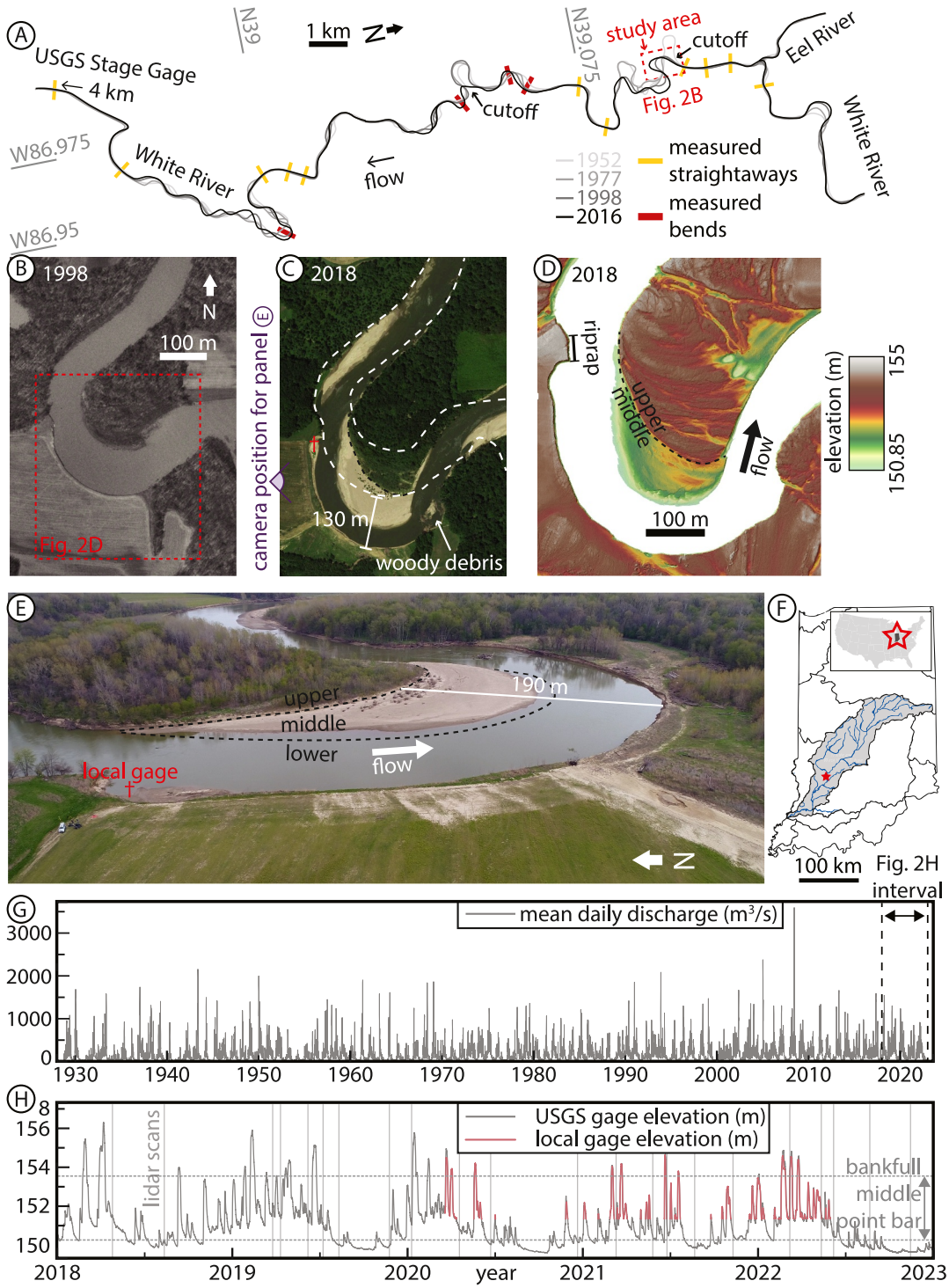

Figure 2. (a) Line tracing of the White River based on four aerial photographs since 1952, with gridlines showing position (latitude longitude). (b) 1998 aerial photograph of the study bend (USGS, 1998). (c) 2018 satellite image, with 1998 banklines and a black dashed line separating the upper and lower point bar. © Google Earth 2023. (d) Lidar map with hillshade. (e) Drone photograph taken 16 April 2020, looking east over the bend (location in (c)). Black dashed lines separate regions of the point bar. (f) Indiana watersheds with the West Fork White River watershed shaded and the study site starred. Adapted from Martin et al. (2016). Inset: Contiguous USA with Indiana marked. (g) Historic hydrograph from the Newberry USGS station. (h) Water elevation between 2018 and 2022, with upper and lower point bar boundary elevations noted. Vertical lines mark drone-based lidar scan dates. Red overlay shows atmospheric-corrected measurements from a local gage installed in early 2020 (daggers in (c, e)).

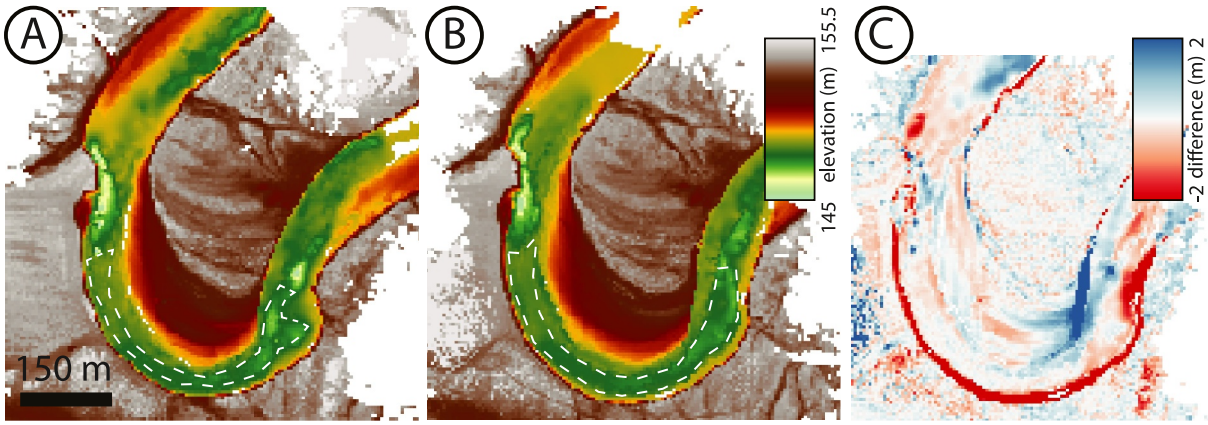

Figure 3. Continuous topography maps from August 2019 (a) and August 2022 (b) created by merging bathymetric maps and drone-based lidar DEMs created from data collected within one day of each other. Cell size is 5 m. (c) DEM-of-Difference (DoD) of (a) and (b).

description of our data collection and processing workflow is provided in the Supporting Information, with additional details available in Martin, Edmonds, Yanites, and Niemi (2024).

We collected bathymetric surveys in August 2019 and August 2022 using a boat-mounted single-beam sonar. Each survey was merged with subaerial drone-based lidar collected the day before or after to create continuous bathymetry-topography maps (Figure 3). The average riverbed elevations in the white dashed polygons of Figures 3a and 3b are 147.94 m for 2019 and 147.98 m for 2022, suggesting no significant change in sediment storage along the channel-bed over the study interval (Figure 3). This indicates channel migration was lateral rather than incisional or aggradational (Figure 1). We also collected grain-size measurements on 17 August 2022. Six samples were taken from the point bar (P1–P6; Figure 4), each from about 10 to 20 cm below the surface, as well as two samples from the cutbank from the muddy upper (C1) and sandy lower (C2) units. A final sample constituted sediment trapped in a stage gage container that was inundated only during flood events (S1). Each sample was dried and sieved to measure the weight of sample fractions across 5 classes ranging from >4 mm (medium gravel) to <250 μm (very fine sand). The upper cutbank and stage gage samples had grain sizes that were too fine to be sieved and were instead analyzed with a Malvern Mastersizer 3000 laser particle-size analyzer. This technique uses laser diffraction to measure the percent distribution (across nine additional classes ranging down to <1 μm) for grain size based on volume instead of mass.

3.2. Change Detection

3.2.1. Point Bar

Changes were measured for each pair of successive lidar scans, which are referred to as events; this term is used with the acknowledgment that some events contained multiple distinct floods. Point bar changes were measured by creating vertical DEMs-of-Difference (DoDs) for target areas of the middle point bar. We separated the point bar into three contiguous domains (Figures 2d and 4). The upper point bar is the area that is vegetated year-round, higher in elevation, and extends to the riverward edge of the riverward-most scrollbar (Figure 2e). The middle point bar is the adjacent, lower-elevation, coarse-grained, sparsely vegetated area that is typically subaerially exposed during low-flow and submerged only during flood events, with a greater portion submerged during larger floods. The lower point bar is the part of the point bar that was usually submerged during our study period (Figure 4c). To create DoDs for each event, the boundary between middle and lower point bar was set as the water-land boundary; areas that were underwater during either scan were unable to be compared and were thus excluded. We measured the volumetric change over the resulting DoDs. However, as each DoD had a different area, we also report these changes normalized to the long-term median middle point bar area observed during our scans, which were usually collected during low-flow periods (Figure 2h). This prevents scans with lower water levels from showing artificially greater changes than those with less bar exposure.

Having many frequent, high-resolution scans allowed us to measure the elevation trajectories of individual points on the middle point bar through time. We performed two such analyses over the intersection of 20 point bar scans;

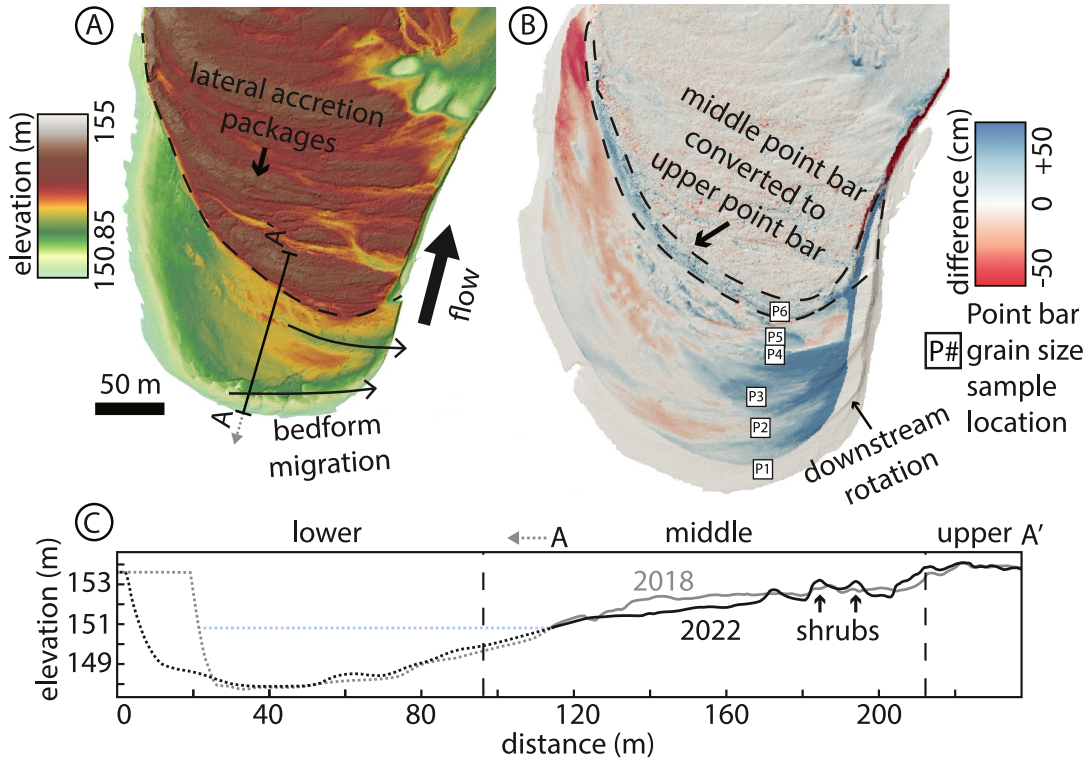

Figure 4. (a) A hillshaded lidar scan of the point bar in April 2018. Black dashed line separates the upper and middle point bar. (b) DoD from December 2020 to November 2022, showing 2 years of topographic change. Sediment sample locations (Figure 5) are shown. (c) Topographic profiles from A to A′, extended to the other bank using DEMs from Figures 3a and 3b. The gray and black solid lines show topography on April 2018 and November 2022, respectively, with bathymetry (from 2019 to 2022 surveys) and water level (April 2018 scan) projected beyond A as dashed lines.

two scans were excluded due to high water levels that obscured most of the middle bar. The first analysis tracks relative elevation through time for 4,258 individual downsampled 4 m^2 square cells. We plotted these trajectories, along with the mean and the 5th and 95th percentiles of their distributions, to visualize spatial variability in erosion and deposition over time. We also plotted the mean aggradation rate of the area of middle point bar that was colonized by vegetation during the study period. The second analysis investigated the timescale over which measurements of aggradation or erosion on point bar surfaces became representative of longer-term rates. To do this, measurements in the same intersection area were downsampled to 1 m^2 cells, resulting in 16,662 points in space. For each of these points we included 20 elevation measurements collected during the study period. For each point, we calculated all 190 unique differences available by comparing observations at each time to all other times, creating 3,158,182 differences in elevation across the polygon. These differences were divided by the time between scans and converted to units of apparent elevation change per year.

3.2.2. Cutbank

We investigated the magnitude, location, and timing of cutbank erosion. Cutbank erosion could not be directly measured using DoDs because of short, dense shrubby vegetation present over parts of the cutbank, particularly in later years. This vegetation resulted in fewer bare-earth points directly atop the cutbank and false ground elevations that varied seasonally on the order of up to 1 m. Instead, we employed three simplifying assumptions: (a) as established through bathymetry and repeat lidar scans, the cutbank floodplain surface and thalweg elevations can be reasonably approximated as uniform and constant, (b) the cutbank migrated laterally while preserving its vertical profile, and (c) each cutbank cell is eroded the first time its elevation drops >1.5 m below the average unvegetated cutbank elevation. We then mapped each eroded cell during each event to its nearest 2 m segment on a smoothed cutbank trendline (dashed line in Figure 9a). Then, areas were converted to volumes by multiplying them by the average height of the cutbank above the thalweg, yielding the total volume of erosion. To make sure that our assumptions accurately capture erosion volumes, we validated this methodology by comparing the total

volume of cutbank erosion measured by the sum of each step in this method to the total volumetric change of the cutbank measured from a DoD of merged bathymetry and topography in August 2019 and August 2022 (Figure 3). Over this period, the cutbank volume change based on this method was 41,100 m^3 compared to 39,421 m^3 measured via merged bathymetry and topography: a difference of less than 6%.

Analogous to our point bar analysis, we also investigated the timescale over which measurements of cutbank retreat became representative of longer-term rates. We separated the cutbank into 20 m intervals and measured apparent retreat rates for all 231 unique differences between the 22 scans. This yielded 9,702 unique erosion rates, which we converted to units of apparent lateral retreat per year.

3.3. Hydrologic Regressions

For each event, volumetric changes were regressed against daily discharge measurements from the Newberry USGS station (Figure 2a). We established that the timing of these discharge data, measured ~20 km away, were consistent with our study site by comparing stage measurements at Newberry to local stage measurements from an atmosphere-corrected pressure transducer installed in the bend in March 2020 (Figures 2c, 2e, and 2h). Using the Newberry USGS station data, we performed two regressions for each event: the mean rate of geomorphic volume change against the maximum daily discharge measurement ($Q_{w,\mathrm{peak}}$), and the total geomorphic volume change against the total flood volume ($V_{w,\mathrm{total}}$). Regressions for point bar and both-bank volumetric changes were performed using both observed and area-scaled point bar changes, with resulting relationships not differing substantially. Total flood volume was calculated by summing all daily flood volumes between two scans, where each daily flood volume is the product of multiplying the daily average discharge by the length of a day. Regressions were also done against total flood volume above a baseflow value, but these results did not differ substantially from total flood volume. We calculated the 95% confidence interval of regression coefficients using the Wald method (The MathWorks Inc, 2023).

4. Results

4.1. Point Bar Deposition

Lidar scans and bathymetric surveys revealed a point bar that sloped downward toward the river with sporadic vegetation on local topographic highs (Figures 4a and 4c). A clear contact separated the sandy middle point bar from the thickly vegetated upper point bar (black dashed lines in Figures 2d and 2e). The middle point bar contained sedimentary structures ranging from plane bedding to dunes that varied from 0.1 to 0.8 m tall, 2–10 m wide, and 1–15 m in wavelength (Figure S6 in Supporting Information S1). These structures were reworked during each inundation. Grain size did not vary much across the middle point bar, consisting mostly of fine gravel and sand (Figure 5). Sediment in the vegetated outermost scroll bar of the upper bar (P6), however, was significantly finer and consisted mostly of grains <250 μm.

While the upper point bar showed minimal change over the study period (Figure 4b), the middle point bar showed considerable and variable volume changes over time (Figure 6a). Both observed and scaled volume changes were erosional over the first half of the study period and depositional over the second half, resulting in a scaled net erosion of 5,300 m^3 (0.23 m average vertical erosion) after four years (Figure 6a). Rates of change between pairs of subsequent observations could be large, ranging from 82 m^3/d of erosion to 40 m^3/d of deposition. Flood magnitude, as measured by either peak discharge or total flood volume, was not a good predictor of the rate of point bar volume change or even whether a given flood was net erosional or depositional (Figures 7a and 7b).

There were only two consistently aggrading areas, each of which was associated with a distinct mechanism of point bar growth (Figure 4b). The first was a band on the inner edge of the middle point bar that was colonized by plants and became a scroll bar, thereby converting into upper point bar over the course of the study period (Figure 4b; green in Figure 8). Nearly all (>99.9%) aggradation rate measurements across all timespans on the sandy point bar surface were slower than the mean aggradation of this colonized emergent scroll bar (Figures 4b, 8a, and 8b). The second area was the downstream end of the point bar, which grew through rotation as sediment was transported via migrating bedforms over the subaerial bartop (Figure 3c; blue in Figure 8; Figure S6 in Supporting Information S1). This resulted in bar accretion surfaces with faces that were parallel with flood-flow and dune trajectories, but nearly perpendicular to the baseflow trajectory. The remaining cells on the point bar experienced an average net erosion of 0.28 m (gold in Figures 8a and 8b). Figure 8b depicts the time and space

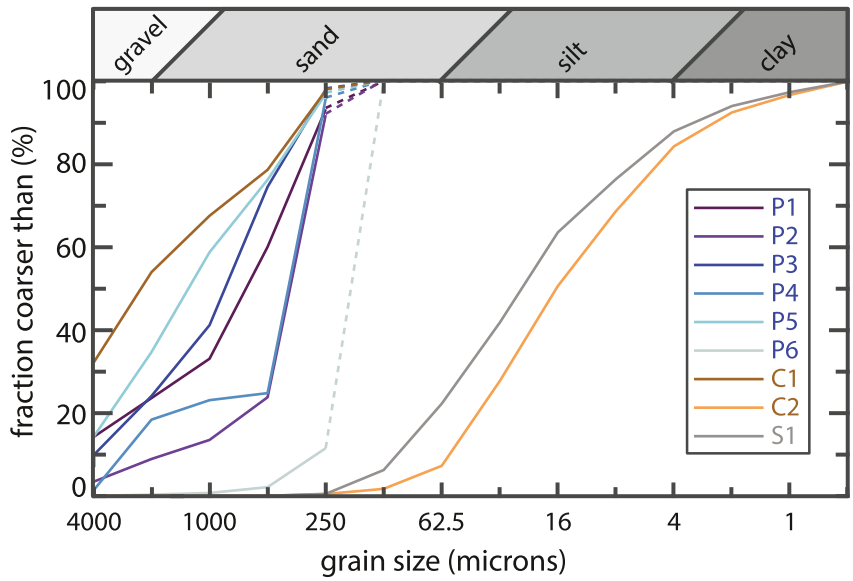

Figure 5. Grain size distribution of sediment samples. Dashed lines indicate fractions smaller than the detection limit of the measurement method. P1 through P6 represent a riverward to landward transect of the point bar (Figure 4). C1 and C2 were taken from the lower and upper cutbank (Figure 9). Sample S1 was recovered from the stage gage housing (Figures 2c and 2e) and was inundated only during floods. C2 and S1 are presented in volume percentage instead of mass percentage.

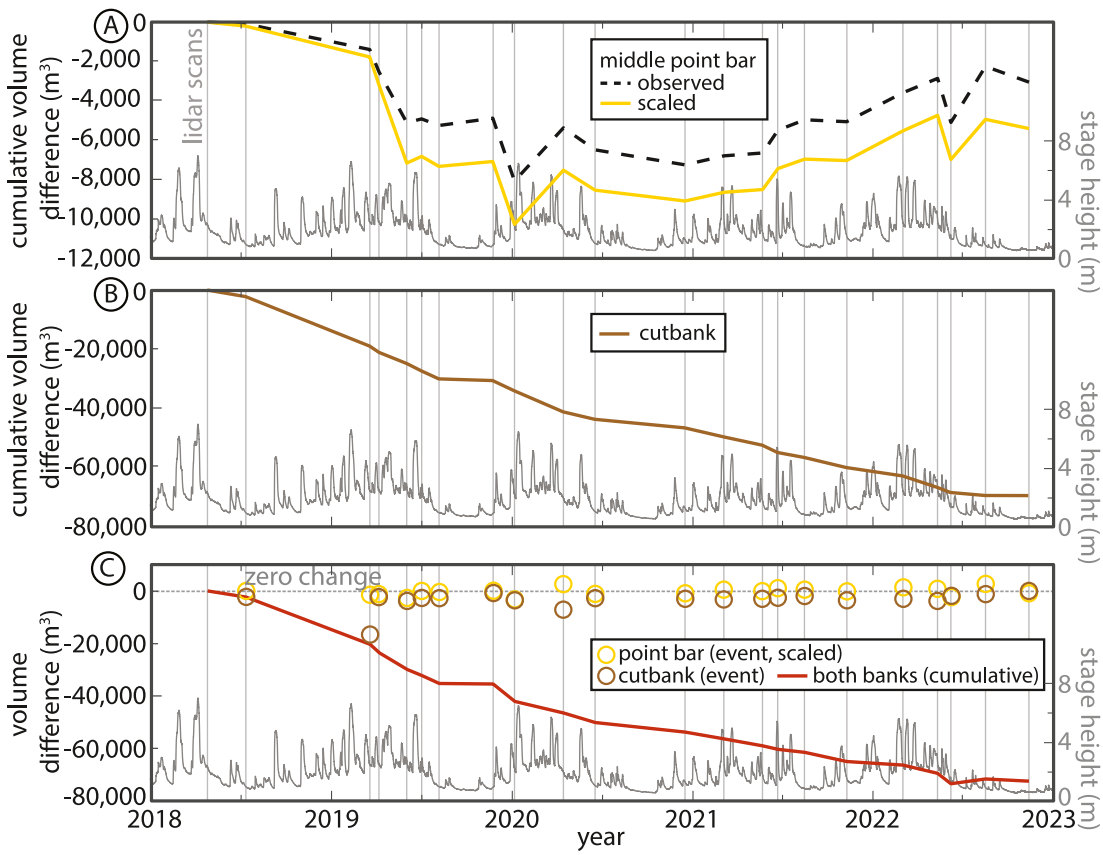

Figure 6. Volume changes through time for the (a) middle point bar (cumulative, observed and scaled), (b) cutbank (cumulative), and (c) both banks (point bar + cutbank). Scan dates and stage gage hydrograph shown to provide context to volumetric changes.

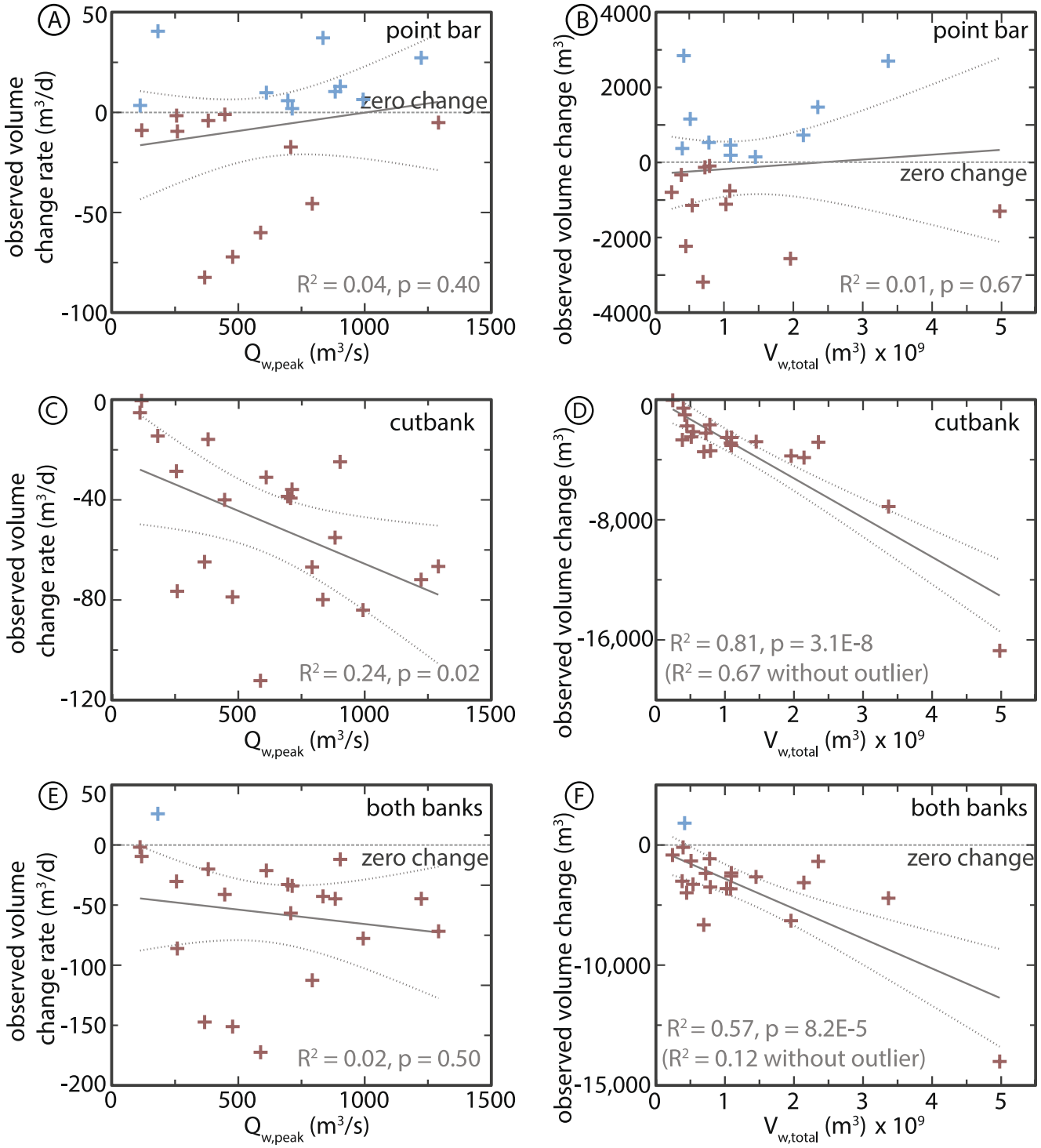

Figure 7. Regressions of geomorphic volume changes against flood measurements. (a, c, e) Peak discharge versus the rate of geomorphic volume change. (b, d, f) Total flood volume versus the total geomorphic volume change. Each cross represents one event. Blue crosses are depositional and red-brown ones are erosional. Solid lines show linear regressions including all measurements (with p-values of slopes; see Table S2, https://zenodo.org/records/11114056 for equations and Spearman rank correlation coefficients). Dashed lines show the 95% confidence interval of regression coefficients.

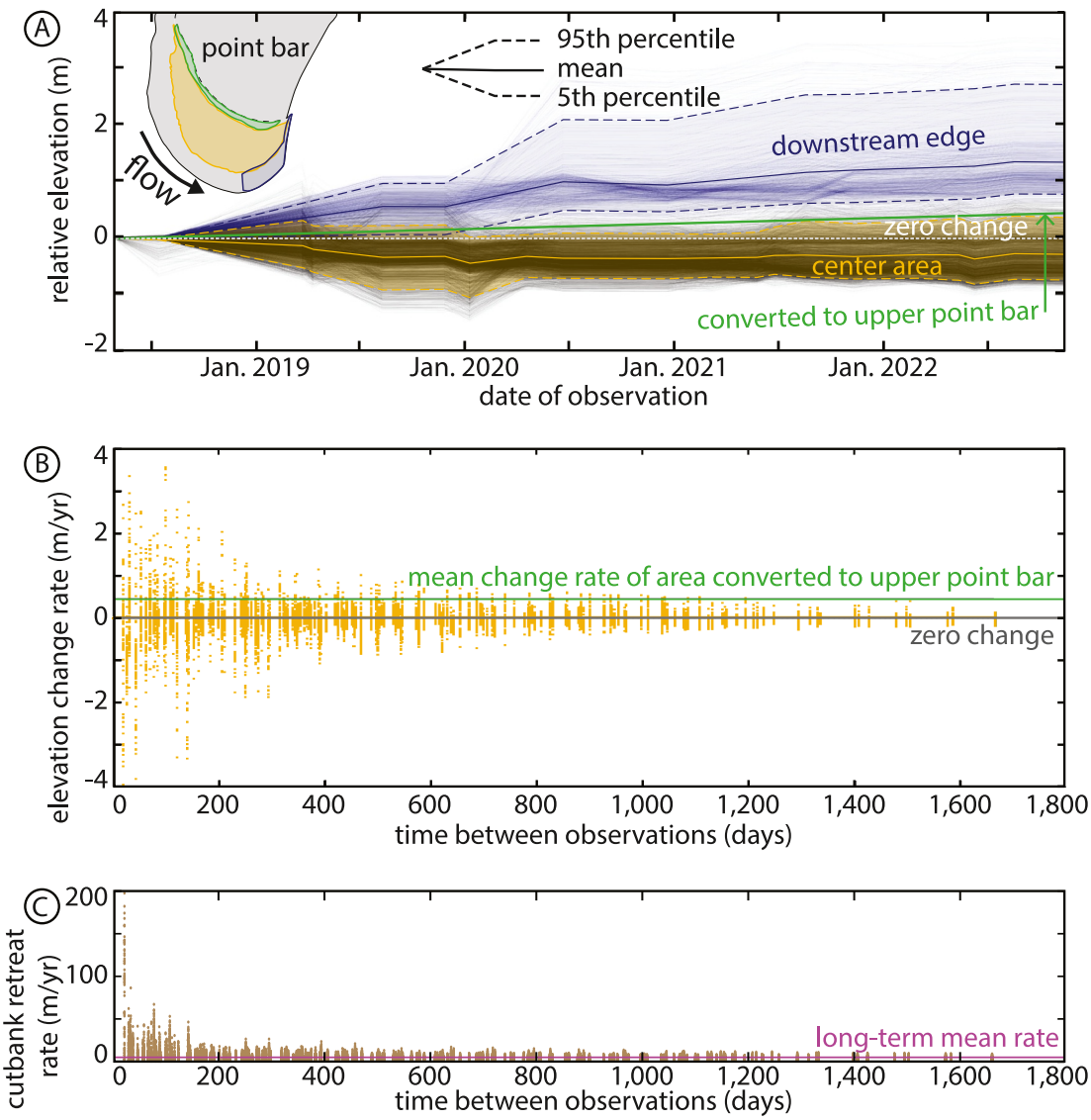

Figure 8. (a) Relative elevation changes over time for areas on the middle (gold, $n = 4{,}258$ cells, each 4 m^2) and downstream (blue, $n = 732$) point bar. The green line shows the mean aggradation rate for cells that were colonized by plants and converted from the middle to upper point bar ($n = 2{,}156$). Inset shows location of gold, blue, and green areas. (b) Apparent aggradation and erosion rates from the gold area as measured across different time intervals ($n = 16{,}662$ cells). Ten outliers are not shown: at 19 days apart, their apparent rates are between −4.3 and −9.6 m/yr. (c) 9,702 apparent cutbank retreat rates for 20 m cutbank reaches measured across different intervals. One outlier is not shown at 19 days apart with a rate of 202.6 m/yr.

variability of apparent erosion or deposition rates measured in this area. While apparent aggradation rates based on measurements collected weeks or months apart could be quite large (>3.5 m/yr), at longer timescales the rates decreased; for any individual point, high frequency but short duration elevation changes on the subaerially exposed point bar surface are rarely representative of longer-term trends.

Even though floods could submerge the entire middle point bar, observed changes to parts of the bar that are normally subaerially exposed between floods are not good predictors of total point bar changes (including parts of the bar that are normally submerged between floods). Merged bathymetry and topography from 2019 to 2022 showed 17,100 m^3 (0.74 m average vertical change) of deposition, while changes on the part of the point bar that was subaerially exposed between floods showed nearly no scaled change (290 m^3 of deposition) over the same period (Figure 3c). This indicates a sedimentological disconnect between domains on point bars that are submerged either perennially or only during floods; the perennially subaqueous part of the point bar sequestered sediment while the part that was only submerged during floods was essentially a bypass zone. Even though

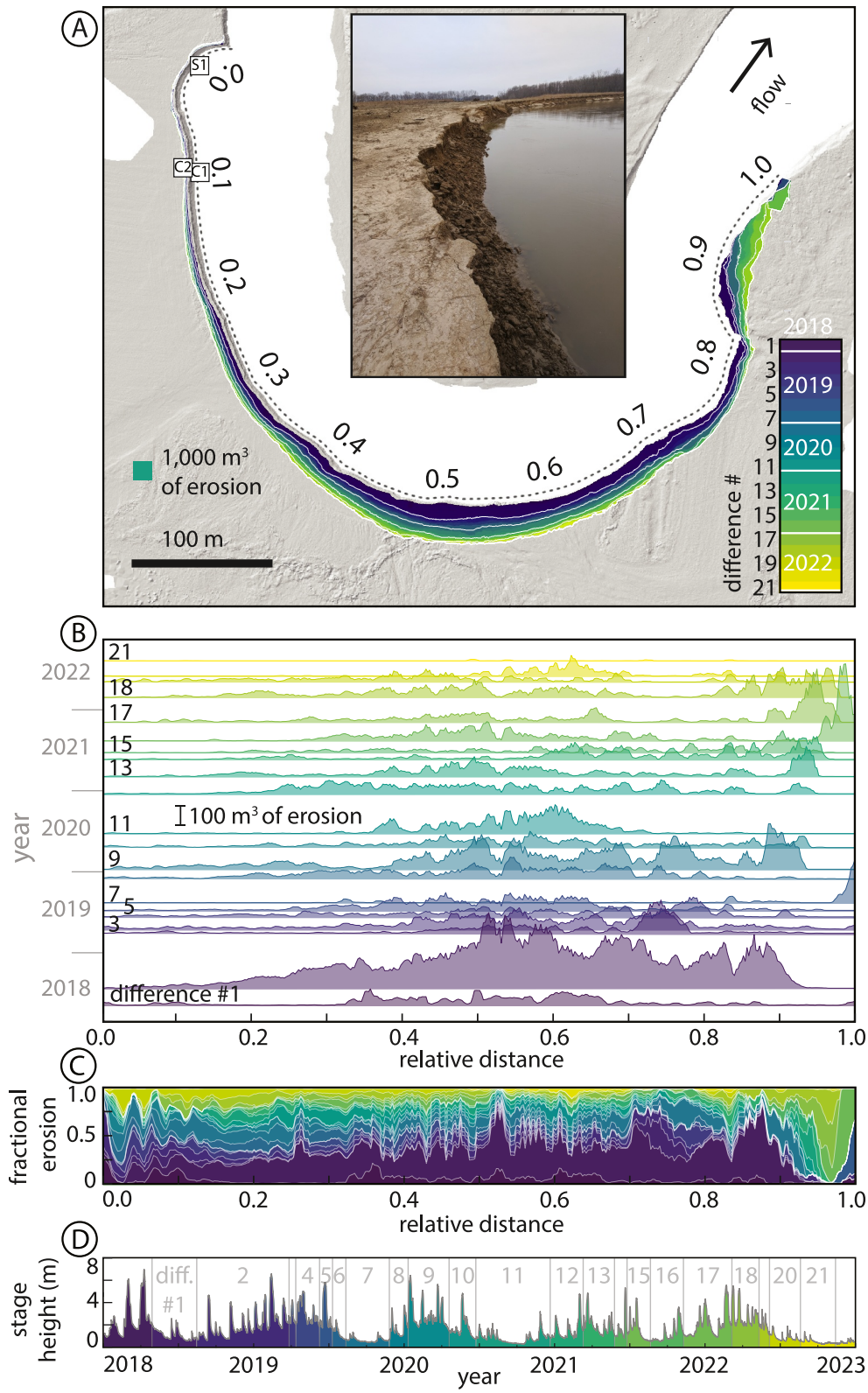

Figure 9.

deposition in this former zone was significant, it was limited to a relatively small area along the meander bend; most of the radial distance of the point bar was net erosional or neutral (Figure 3).

4.2. Cutbank Erosion

Much of the cutbank was covered by short, dense shrubs that varied seasonally. The top meter or so of the cutbank was primarily silt and clay soil and had been used for crop growth since at least 1952 (see Figures S1–S5 in Supporting Information S1). This more-resistant material was underlain by sandy and gravelly unconsolidated sediments (Figure 5) that featured both dune-scale and bar-scale cross-bedding. The unconsolidated material that made up most of the cutbank had a very similar grain size profile to the modern middle point bar samples. Overbank deposition on the cutbank was mainly limited to cm-thick sand sheets advected a few meters away from the channel. This process would presumably form levees if the cutbank migrated slower, but here cutbank erosion returns this sediment to the channel before substantial relief can be generated. The main mechanism of cutbank erosion was the removal of unconsolidated sediments beneath the resistant muddy upper material, causing upper bank failure and resulting in muddy slump blocks that could drape the sandy cutbank beneath. Erosion tended to result in scallop-shaped features that were meters to tens of meters wide (Figure 9a, inset photo). The total volume eroded from the cutbank over the study period was 69,500 m^3 (Figure 6b). The rates of cutbank erosion varied considerably per scan, from 0.45 m^3/d to 112 m^3/d. These changes depended on flood magnitude and correlated more strongly with the total (Figure 7d, $R^2 = 0.81$) discharge over a given period of measurement compared to the maximum (Figure 7c, $R^2 = 0.24$). Some of this former trend was affected by a large outlier event that encompassed the first half of the 2018–2019 hydrologic year; total flood volume fit was $R^2 = 0.67$ with the outlier removed.

The location of maximum cutbank erosion varied along the bank through time. While the distribution of erosion was roughly continuous over annual or interannual timescales (Figure 9a), cutbank erosion was both dynamic and non-uniform on shorter timescales (Figure 9b). While some events caused widespread erosion, most events had distinct pockets of erosion (Figure 9b). Hiatuses in erosion were common, where significant erosion events would be followed by prolonged periods of non-erosion (brighter white lines in 9C). For example, the area around 75% of the distance along the cutbank was strongly erosional during the first half of the study period but waned to nearly no erosion during the second half (Figures 9b and 9c). Conversely, the region beyond 90% of the distance along the cutbank experienced little erosion during the first half of the study period but had an erosional front move downstream through the second half of the study period. Like the point bar, apparent cutbank retreat rates were highly variable when calculated using short measurement intervals (Figure 8c).

4.3. Net Bend Change

Point bar deposition was less than cutbank erosion over the study period, leading to net erosion across the bend (red line in Figure 6c). When including both subaqueous and subaerial changes, we observed 17,110 m^3 of total point bar deposition against 39,420 m^3 of cutbank erosion for the period covered by bathymetry (August 2019 to August 2022), for a net loss between both banks of 22,310 m^3. This imbalance between banks is greater than is typically expected from overbank deposition and geometric extension alone (Lauer & Parker, 2008). In other words, we do not observe evidence that this meander bend has been able to conserve mass and compensate its own widening over our observation window.

Similarly to the point bar, both-bank volume change rates were poorly predicted by peak discharge (Figures 7e and 7f). Net volume changes appeared to vary with total flood volume, but these relationships became insignificant when the single large outlier was removed (Figure 7f). Any predictive strength in this relationship is likely due to the relationship between cutbank erosion and flood magnitude. The same regressions were

Figure 9. Patterns of cutbank erosion through space and time, where each color corresponds to erosion observed between a different pair of subsequent scans. (a) Planform map of cutbank erosion. Erosion is converted from area to volume using an assumed uniform thickness; see Methods. Inset: Field photo of the cutbank, standing on the south shore looking upstream at an unvegetated part of the cutbank. Photo was taken during relatively high water levels shortly after bank collapse while muddy slump blocks still armor underlying unconsolidated sediments. For scale, the water level was approximately 2 m below the top of the cutbank. (b) Cutbank erosion versus distance along the cutbank. Erosion curves are smoothed with a moving window mean of 10 m. (c) Relative cutbank erosion map with *y*-axis erosion units scaled by the total amount of erosion each area experienced. White semi-transparent lines represent boundaries between scans; closely spaced white lines appear brighter and represent longer hiatuses. (d) USGS hydrograph from Figure 2h, colored by time, with differences between lidar scans labeled.

performed on the sum of the absolute values of point bar and cutbank changes with similar results (see Figure S7 in Supporting Information S1).

5. Discussion

5.1. Dynamics of Deposition and Erosion

The high temporal and spatial resolution record of erosion and deposition in this study allows for detailed analyses of individual changes on a meandering river bend. This satisfies recent calls for both the importance of considering the motion of the inner and outer banks independently, and for increased spatial and temporal resolution of landscape change measurements (Donovan & Belmont, 2019; Donovan et al., 2021; Eke et al., 2014; Mason & Mohrig, 2019).

When investigating changes to point bars or cutbanks, a sensible place to start is determining the temporal period over which to measure migration or erosion rates. Over short timescales, measured apparent rates are noisy (Figures 8b and 8c). The apparent aggradation and erosion rates of both the cutbank and middle point bar declined when measured over longer intervals, consistent with theory and previous observations over significantly longer timescales (Donovan & Belmont, 2019; Nanson & Hickin, 1983; Sadler, 1981; Schumer & Jerolmack, 2009). However, apparent cutbank erosion rates approached their long-term means faster than apparent point bar vertical change rates approached their long-term averages (Figures 8b and 8c). In other words, changes measured over the scale of 4–10 months are more representative of long-term trends for cutbanks than for middle point bars. For both point bar and cutbank measurements, our observation window of 4 years exceeds the noisiest of the short-term rates (Figures 8b and 8c).

We then investigated the dynamics of point bar deposition. The only component of the point bar that migrated toward the cutbank was the landward boundary of the middle point bar. Over the study period, sediment deposited here was colonized by plants and ultimately converted into upper point bar as the outermost scroll bar (Weisscher et al., 2019; Zen et al., 2017). Vegetation can induce net deposition once achieving a critical growth state, but the sediment can be re-eroded away if flooding occurs before seeds develop strong root structures (Braudrick et al., 2009; Bywater-Reyes et al., 2017; Rominger et al., 2010). An important driver of bar-push, then, should be the ratio between the time needed for vegetation to colonize and stabilize sediments and the return interval of a flood capable of re-eroding those sediments; modeling suggests that single-threaded rivers with highly sinuous narrow channels preferentially form when this ratio is small (less than about 0.1; Asahi et al., 2013). In this scenario, sediment trapped by vegetation on the point bar rapidly narrows the channel by moving the inward boundary toward the cutbank, deflecting flow and forcing erosion (Constantine et al., 2014; Dietrich & Smith, 1984; Dietrich et al., 1979; Lewin, 1976). We do not see this at our study site, as cutbank erosion happens far more quickly than inner bank accretion (banks in Figure 4c). Perhaps at our site slow plant colonization timescales have established a maximum point bar migration rate that is too slow to match the rate of cutbank erosion. This would further suggest a biological control on whether bend migration is driven by bar-push or bank-pull and should be testable by comparing point bar migration rates between biomes, including Arctic rivers with permafrost in their floodplains where vegetation has been interpreted to slow lateral migration rates (Ielpi et al., 2023).

5.2. River Width Maintenance: Bar-Push or Bank-Pull?

We see no evidence for a systematic trend in overall net deposition or erosion with varying flood intensities once the large outlying flood is removed (Figures 7e and 7f). As such, our findings do not align with previous research (ex. Asahi et al., 2013; Grams et al., 2020; Pizzuto, 1994) that suggested smaller floods lead to channel narrowing (by preferentially depositing on point bars) while larger floods favor channel widening (by preferentially eroding cutbanks). In nearly all events, the meander bend studied here was net erosional, both on the intra- and interannual timescales (Figures 7e and 7f). While our observation window was shorter than Pizzuto (1994) on the Powder River, the White River experienced a variety of flood sizes, including many small floods, which previous findings indicate should have been the most aggradational. Further, the bend did not experience extreme events, which should have been the most erosional, compared to the previous 100 years recorded by the local gauging station (Figure 2g).

It has been suggested that bar push and bank pull can be distinguished from one another by observing changes in channel width over time. More specifically, observations that the inner or outer bank moves faster than the other over some measurement period, or observations of overall net erosion or deposition in the bend, have both been used to interpret bar-push or bank-pull as river migration mechanisms respectively (Eke et al., 2014; Mason & Mohrig, 2018; Parker et al., 2011). However, we argue that channel widening is not a unique identifier of bank-pull, nor is channel narrowing unique to bar-push. Consider an initial river bend with a channel width at a long-term equilibrium. Now, consider a perturbation that occurs on this bend, beginning a single bar-push or bank-pull cycle by forcing the width to deviate from the long-term equilibrium. For bar-push, the river initially narrows due to point bar deposition, before widening from cutbank erosion as it relaxes back toward equilibrium. For bank-pull, widening from cutbank erosion is followed by narrowing from point bar deposition. In both cases, the cycle would contain phases of widening, but on different limbs of the response as either perturbations or responses (compare points i and ii in Figure 10a). This issue with identification persists even if multiple bar-push or bank-pull events were to follow one another in succession, such as would be expected from a continually migrating river. In this case, we could observe identical narrowing-to-widening or widening-to-narrowing patterns whether width were being maintained by bar-push or bank-pull. For example, observing narrowing-to-widening could equally indicate a full bar-push cycle, or the response of a prior bank-pull cycle followed by the initiation of another bank-pull cycle.

While it may not be possible to distinguish between bar-push or bank-pull by observing widening or narrowing alone, we argue that these should be distinguishable by instead measuring changes in width relative to the equilibrium, pre-perturbation width of the river between events. For example, if the river width is consistently smaller than the equilibrium width whether it is widening or narrowing, the river is in the bar-push domain (Figure 10a). Accordingly, knowing the equilibrium width of a river provides a method to distinguish whether a particular motion (i.e., widening or narrowing) is a perturbation or a response, and thus a means to distinguish between bar push and bank pull in natural settings. It bears noting that this approach presupposes that an equilibrium steady river width occurs between events. Contrarily, imagine the case where the width of a river is tracked over a long timescale, but width continually and indefinitely oscillates between widening and narrowing without ever equilibrating (Figure 10b). While this is not predicted by modeling (Eke et al., 2014), in such a case, bar-push or bank-pull would not be meaningfully distinct as neither bank's motion can be said to have initiated the cycle. Measuring any subsequent widening then narrowing, or vice versa, would be purely dependent on when the observer chooses to observe, and thus bar-push and bank-pull would lose physical meaning as distinct ways for rivers to maintain width.

We applied our suggested strategy for distinguishing between bar-push and bank-pull to our own data set by first looking for an equilibrium, pre-perturbation width during our observation window. Rather than an equilibrium width, we found that the meander bend studied here progressively widened throughout the study period because the cutbank retreated faster than the point bar advanced (Figure 10c). This trend holds whether measuring bankfull width, defined as equal elevation points from the cutbank to the outermost scroll-bar (Mason & Mohrig, 2018), or widths at fixed elevations below the floodplain (Mason & Mohrig, 2019; Figure 10d). While these latter widths should be less dependent on vegetation encroachment rates as they measure the distance between points on unconsolidated sediment surfaces, we still observed channel widening at all measured elevations.

Not finding an equilibrium width during our observation window, we considered that the entire study period may have been part of a widening limb of a decadal-scale bar-push or bank-pull cycle (i or ii in Figure 10a; Mason & Mohrig, 2019) and so looked for an equilibrium river width in historical aerial photographs. Instead, we found that after the initiation of migration after a cutoff sometime between 1965 and 1970, the bend-averaged width has increased from 90 m in 1977 to 122 m in 1998 (1.51 m/yr average) to 144 m in 2018 (1.11 m/yr) and then to 151 m in 2022 (1.58 m/yr). We have no evidence to suggest that this bend has ever had an equilibrium, steady river width between widening-and-narrowing cycles; instead, it appears to have widened continuously since migration began. To validate that this is not an artifact of the river as a whole widening, we measured 10 straightaway widths up and downstream of the bend using aerial photographs between 1952 and 2016 (Figure 2a). Of these, bends widened at an average rate of 0.08 m/yr, with three straightaways having narrowed. We also compared the meander bend studied here to four other nearby bends that have similar land use and land cover (Figure 2a). These widened at an average rate of 0.26 m/yr, with one narrowing; widening was slower on average than the bend over which we collected lidar scans, but faster than the straightaways. One reason that the bend studied here may have widened

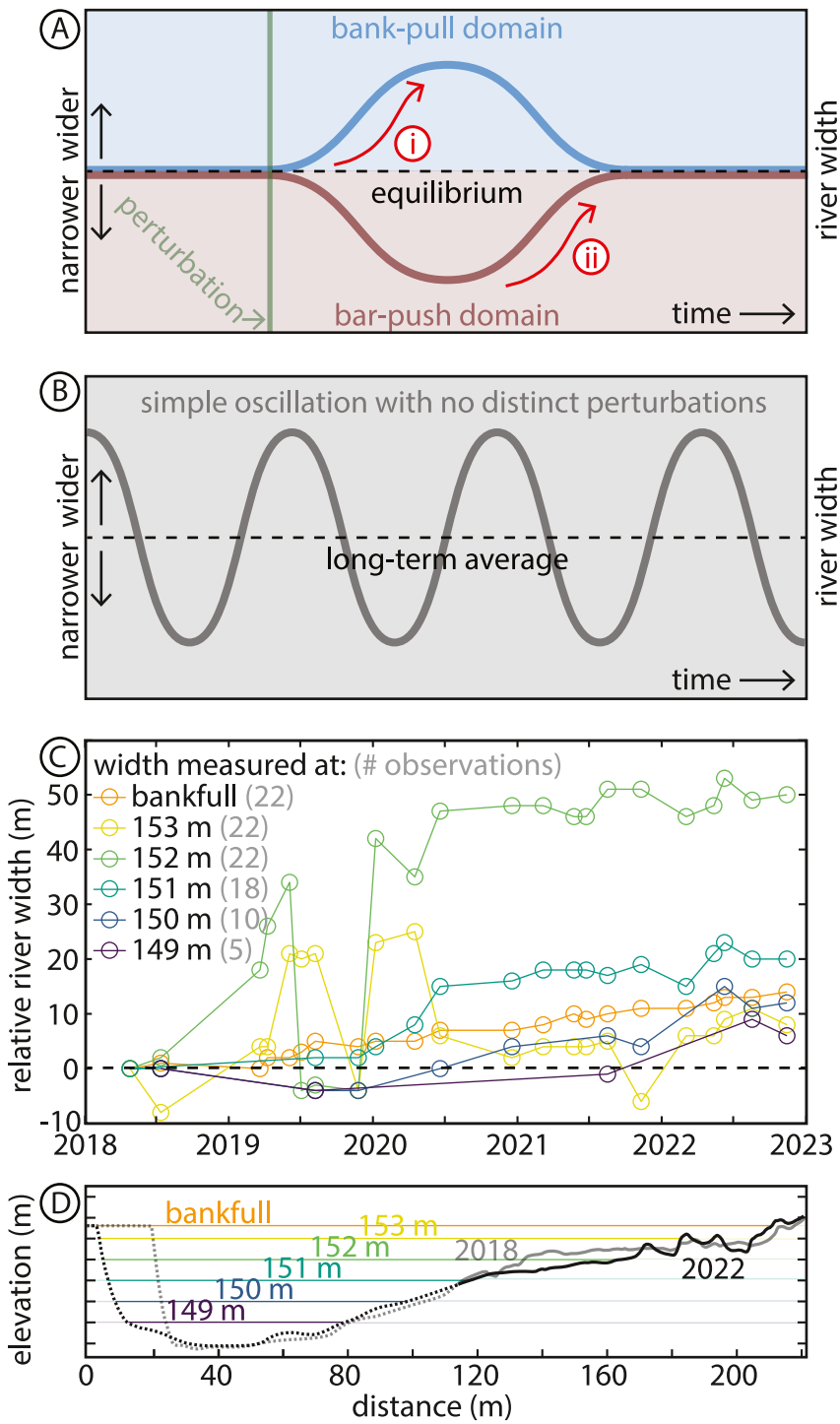

Figure 10. (a) Individual changes in width alone (ex. widening in (i) and (ii)) cannot distinguish between bar-push and bank-pull unless an equilibrium width is known. (b) If there is no equilibrium width, bar-push and bank-pull are not meaningfully distinct because widening or narrowing do not move to or away from a specific width. (c) Observed river widths over time at different elevations for our study bend. Due to the rarity of observing the river at 149 m, three measurements were included for elevations up to 149.15 m. (d) Elevations at which measurements were taken for (c).

so quickly compared to the other four is because we are measuring after a cutoff that occurred ~55 years ago (Figure 2a). A cutoff should result in an abrupt local increase in slope and curvature, both of which could increase shear stress on the cutbank (Donovan et al., 2021; Monegaglia & Tubino, 2019). However, while post-cutoff widening was observed in a global remote sensing study by Lopez Dubon and Lanzoni (2019), it tended to disappear within a few years after the cutoff. Similarly, Schwenk and Foufoula-Georgiou (2016) observed channel widening in nearby meander bends after the 1997 Masisea cutoff on the Ucayali River in the Amazon Basin, but these bends generally returned to normal widths within 5–10 years rather than the decades we have observed.

The continuous widening of the meander bend in our study area may have traditionally be interpreted as observing bank-pull as a mechanism for river migration, since the cutbank has migrated in the apparent absence of point bar accretion. However, despite 22 high-resolution bare earth DEMs of a single actively migrating point bar and cutbank, collected at nearly a flood-scale frequency, we do not observe evidence for either bar-push or bank-pull as mechanisms for maintaining river width. In fact, we observe evidence that neither is at work; this meander bend is not maintaining width, and has not, over the last ~55 years.

6. Conclusions

We present a data set consisting of 22 repeat drone-based lidar surveys of a single paired point bar and cutbank (~0.35 km^2 in area) over 4.5-years. There was net erosion from the subaerially exposed point bar but net deposition from the subaqueous point bar, which indicates these regimes can evolve independently. Cutbank erosion over interannual timescales was roughly continuous but occurred in spatially discrete scalloped chunks over flood timescales. Overall the bend was net erosional as point bar deposition was significantly less than cutbank erosion, leading to continual channel widening over the bend's ~55 year lifespan to-date. This is evidence that neither bar-push nor bank-pull act to maintain width in this meander bend. Finally, we suggest that resolving the difference between bar-push and bank-pull events as mechanisms for river width maintenance using observations of width changes in natural rivers requires an advancement of current theory, but could be solved by determining the equilibrium width of meandering river bends.

Data Availability Statement

Summary volumetrics, grain size measurements for sediment samples, stream gauge data for the Newberry USGS station, and equations for hydrologic regressions with statistical measures are all included in Tables S1–S6. All 22 of the drone-based lidar DEMs have been created with unified spatial reference systems and resolutions. These tables and DEMs are available in Martin, Edmonds, and Lewis (2024).

Acknowledgments
We would like to thank editor Amy East, associate editor Marisa Repasch, two anonymous reviewers, and Alvise Finotello for helpful and insightful comments that have improved this manuscript. We would also like to thank our drone pilot Steve Scott, as well as Eric Barefoot, Jenna Bazzell, Jaxon Bennett, Connor Broaddus, Tyler Doane, James Gearon, Eduardo L. González Lugo, Riley Henson, Dylan Lee, Garrett Marietta, Ben Peters, and Jeffrey Valenza for assistance with fieldwork and/or sample processing. HKM was supported by National Aeronautics and Space Administration (NASA) Future Investigators in NASA Earth and Space Science and Technology (FINESST) Grant 80NSSC21K1598, an International Association of Sedimentologists Postgraduate Research Grant, and a California Institute of Technology Geological and Planetary Sciences Geology Option Postdoctoral position. DAE was supported by National Sciences Foundation Grant EAR-2321056. QWL was supported by a University of Waterloo New Faculty Starter Grant. All authors were supported by the Environmental Resilience Institute, funded by Indiana University's Prepared for Environmental Change Grand Challenge initiative.

References

Asahi, K., Shimizu, Y., Nelson, J., & Parker, G. (2013). Numerical simulation of river meandering with self-evolving banks. *Journal of Geophysical Research: Earth Surface*, *118*(4), 2208–2229. https://doi.org/10.1002/jgrf.20150

Braudrick, C. A., Dietrich, W. E., Leverich, G. T., & Sklar, L. S. (2009). Experimental evidence for the conditions necessary to sustain meandering in coarse-bedded rivers. *Proceedings of the National Academy of Sciences*, *106*(40), 16936–16941. https://doi.org/10.1073/pnas.0909417106

Bywater-Reyes, S., Wilcox, A. C., & Diehl, R. M. (2017). Multiscale influence of woody riparian vegetation on fluvial topography quantified with ground-based and airborne lidar. *Journal of Geophysical Research: Earth Surface*, *122*(6), 1218–1235. https://doi.org/10.1002/2016JF004058

Constantine, J. A., Dunne, T., Ahmed, J., Legleiter, C., & Lazarus, E. D. (2014). Sediment supply as a driver of river meandering and floodplain evolution in the Amazon Basin. *Nature Geoscience*, *7*(12), 899–903. https://doi.org/10.1038/ngeo2282

Corenblit, D., Vautier, F., González, E., & Steiger, J. (2020). Formation and dynamics of vegetated fluvial landforms follow the bio-geomorphological succession model in a channelized river. *Earth Surface Processes and Landforms*, *45*(9), 2020–2035. https://doi.org/10.1002/esp.4863

David, S. R., Edmonds, D. A., & Letsinger, S. L. (2017). Controls on the occurrence and prevalence of floodplain channels in meandering rivers. *Earth Surface Processes and Landforms*, *42*(3), 460–472. https://doi.org/10.1002/esp.4002

Dietrich, W. E., & Smith, J. D. (1984). Bed load transport in a river meander. *Water Resources Research*, *20*(10), 1355–1380. https://doi.org/10.1029/WR020i010p01355

Dietrich, W. E., Smith, J. D., & Dunne, T. (1979). Flow and sediment transport in a sand bedded meander. *The Journal of Geology*, *87*(3), 305–315. https://doi.org/10.1086/628419

Donovan, M., & Belmont, P. (2019). Timescale dependence in river channel migration measurements. *Earth Surface Processes and Landforms*, *44*(8), 1530–1541. https://doi.org/10.1002/esp.4590

Donovan, M., Belmont, P., & Sylvester, Z. (2021). Evaluating the relationship between meander-bend curvature, sediment supply, and migration rates. *Journal of Geophysical Research: Earth Surface*, *126*(3), e2020JF006058. https://doi.org/10.1029/2020JF006058

Douglas, M. M., Miller, K. L., Schmeer, M. N., & Lamb, M. P. (2023). Ablation-limited erosion rates of permafrost riverbanks. *Journal of Geophysical Research: Earth Surface*, *128*(8), e2023JF007098. https://doi.org/10.1029/2023JF007098

Eke, E., Parker, G., & Shimizu, Y. (2014). Numerical modeling of erosional and depositional bank processes in migrating river bends with self-formed width: Morphodynamics of bar push and bank pull. *Journal of Geophysical Research: Earth Surface*, *119*(7), 1455–1483. https://doi.org/10.1002/2013JF003020

Federici, B., & Paola, C. (2003). Dynamics of channel bifurcations in noncohesive sediments. *Water Resources Research*, *39*(6), 1162. https://doi.org/10.1029/2002WR001434

Federici, B., & Seminara, G. (2003). On the convective nature of bar instability. *Journal of Fluid Mechanics*, *487*, 125–145. https://doi.org/10.1017/s0022112003004737

Furbish, D. J. (1988). River-bend curvature and migration: How are they related? *Geology*, *16*(8), 752–755. https://doi.org/10.1130/0091-7613(1988)016<0752:RBCAMH>2.3.CO;2

Gabet, E. J. (1998). Lateral migration and bank erosion in a saltmarsh tidal channel in San Francisco Bay, California. *Estuaries*, *21*(4), 745–753. https://doi.org/10.2307/1353278

Grams, P. E., Dean, D. J., Walker, A. E., Kasprak, A., & Schmidt, J. C. (2020). The roles of flood magnitude and duration in controlling channel width and complexity on the Green River in Canyonlands, Utah, USA. *Geomorphology*, *371*, 107438. https://doi.org/10.1016/j.geomorph.2020.107438

Gurnell, A. (2014). Plants as river system engineers. *Earth Surface Processes and Landforms*, *39*(1), 4–25. https://doi.org/10.1002/esp.3397

Hasegawa, K. (1977). Computer simulation of the gradual migration of meandering channels. In *Proceedings of the Hokkaido Branch* (pp. 197–202). Japan Society of Civil Engineering.

Hickin, E. J. (1984). Vegetation and river channel dynamics. *The Canadian Geographer / Le Géographe Canadien*, *28*(2), 111–126. https://doi.org/10.1111/j.1541-0064.1984.tb00779.x

Ielpi, A., Lapôtre, M. G. A., Finotello, A., & Roy-Léveillée, P. (2023). Large sinuous rivers are slowing down in a warming Arctic. *Nature Climate Change*, *13*(4), 375–381. https://doi.org/10.1038/s41558-023-01620-9

Ielpi, A., Lapôtre, M. G. A., Gibling, M. R., & Boyce, C. K. (2022). The impact of vegetation on meandering rivers. *Nature Reviews Earth & Environment*, *3*(3), 165–178. https://doi.org/10.1038/s43017-021-00249-6

Ikeda, S., Parker, G., & Sawai, K. (1981). Bend theory of river meanders. Part 1. Linear development. *Journal of Fluid Mechanics*, *112*, 363–377. https://doi.org/10.1017/S0022112081000451

Lapôtre, M. G. A., Ielpi, A., Lamb, M. P., Williams, R. M. E., & Knoll, A. H. (2019). Model for the formation of single-thread rivers in barren landscapes and implications for pre-Silurian and Martian fluvial deposits. *Journal of Geophysical Research: Earth Surface*, *124*(12), 2757–2777. https://doi.org/10.1029/2019JF005156

Lauer, J. W., & Parker, G. (2008). Net local removal of floodplain sediment by river meander migration. *Geomorphology*, *96*(1–2), 123–149. https://doi.org/10.1016/j.geomorph.2007.08.003

Lewin, J. (1976). Initiation of bed forms and meanders in coarse-grained sediment. *GSA Bulletin*, *87*(2), 281–285. https://doi.org/10.1130/0016-7606(1976)87<281:IOBFAM>2.0.CO;2

Lightbody, A. F., Kui, L., Stella, J. C., Skorko, K. W., Bywater-Reyes, S., & Wilcox, A. C. (2019). Riparian vegetation and sediment supply regulate the morphodynamic response of an experimental stream to floods. *Frontiers in Environmental Science*, *7*, 40. https://doi.org/10.3389/fenvs.2019.00040

Lopez Dubon, S., & Lanzoni, S. (2019). Meandering evolution and width variations: A physics-statistics-based modeling approach. *Water Resources Research*, *55*(1), 76–94. https://doi.org/10.1029/2018WR023639

Martin, G. R., Fowler, K. K., & Arihood, L. D. (2016). Estimating selected low-flow frequency statistics and harmonic-mean flows for ungaged, unregulated streams in Indiana. *U.S. Geological Survey Scientific Investigations Report 2016-5102* (p. 45). https://doi.org/10.3133/sir20165102

Martin, H. K., Edmonds, D. A., & Lewis, Q. W. (2024). Lidar Scans of the White River near Worthington, Indiana, U.S.A.: Supporting data for Martin et al. (Version 2.1) [Dataset]. *Zenodo*. https://doi.org/10.5281/zenodo.11114056

Martin, H. K., Edmonds, D. A., Yanites, B. J., & Niemi, N. A. (2024). Quantifying landscape change following catastrophic dam failures in Edenville and Sanford, Michigan, USA. *Earth Surface Processes and Landforms*, 1–12. https://doi.org/10.1002/esp.5855

Mason, J., & Mohrig, D. (2018). Using time-lapse lidar to quantify river bend evolution on the meandering coastal Trinity River, Texas, USA. *Journal of Geophysical Research: Earth Surface*, *123*(5), 1133–1144. https://doi.org/10.1029/2017JF004492

Mason, J., & Mohrig, D. (2019). Differential bank migration and the maintenance of channel width in meandering river bends. *Geology*, *47*(12), 1136–1140. https://doi.org/10.1130/G46651.1

Monegaglia, F., & Tubino, M. (2019). The hydraulic geometry of evolving meandering rivers. *Journal of Geophysical Research: Earth Surface*, *124*(11), 2723–2746. https://doi.org/10.1029/2019JF005309

Nanson, G. C., & Hickin, E. J. (1983). Channel migration and incision on the Beatton River. *Journal of Hydraulic Engineering*, *109*(3), 327–337. https://doi.org/10.1061/(ASCE)0733-9429(1983)109:3(327)

NOAA NCEI (National Oceanic and Atmospheric Administration National Centers for Environmental Information). (2023). Divisional time series. Retrieved from https://www.ncei.noaa.gov/access/monitoring/climate-at-a-glance/divisional/time-series

Parker, G., Shimizu, Y., Wilkerson, G. V., Eke, E. C., Abad, J. D., Lauer, J. W., et al. (2011). A new framework for modeling the migration of meandering rivers. *Earth Surface Processes and Landforms*, *36*(1), 70–86. https://doi.org/10.1002/esp.2113

Pizzuto, J. E. (1994). Channel adjustments to changing discharges, Powder River, Montana. *GSA Bulletin*, *106*(11), 1494–1501. https://doi.org/10.1130/0016-7606(1994)106<1494:CATCDP>2.3.CO;2

Rominger, J. T., Lightbody, A. F., & Nepf, H. M. (2010). Effects of added vegetation on sand bar stability and stream hydrodynamics. *Journal of Hydraulic Engineering*, *136*(12), 994–1002. https://doi.org/10.1061/(ASCE)HY.1943-7900.0000215

Sadler, P. M. (1981). Sediment accumulation rates and the completeness of stratigraphic sections. *The Journal of Geology*, *89*(5), 569–584. https://doi.org/10.1086/628623

Schumer, R., & Jerolmack, D. J. (2009). Real and apparent changes in sediment deposition rates through time. *Journal of Geophysical Research*, *114*(F3), F00A06. https://doi.org/10.1029/2009JF001266

Schwenk, J., & Foufoula-Georgiou, E. (2016). Meander cutoffs nonlocally accelerate upstream and downstream migration and channel widening. *Geophysical Research Letters*, *43*(24), 12437–12445. https://doi.org/10.1002/2016GL071670

Smith, C. E. (1998). Modeling high sinuosity meanders in a small flume. *Geomorphology*, *25*(1), 19–30. https://doi.org/10.1016/S0169-555X(98)00029-4

Stott, T. (1997). A comparison of stream bank erosion processes on forested and moorland streams in the Balquhidder Catchments, central Scotland. *Earth Surface Processes and Landforms*, *22*(4), 383–399. https://doi.org/10.1002/(SICI)1096-9837(199704)22:4<383::AID-ESP695>3.0.CO;2-4

Sylvester, Z., Durkin, P., & Covault, J. A. (2019). High curvatures drive river meandering. *Geology*, *47*(3), 263–266. https://doi.org/10.1130/G45608.1

Tal, M., & Paola, C. (2010). Effects of vegetation on channel morphodynamics: Results and insights from laboratory experiments. *Earth Surface Processes and Landforms*, *35*(9), 1014–1028. https://doi.org/10.1002/esp.1908

The MathWorks, Inc. (2023). Confidence intervals of coefficient estimates of linear regression model—MATLAB coefCI. Retrieved from https://www.mathworks.com/help/stats/linearmodel.coefci.html

Thorne, C. R., & Tovey, N. K. (1981). Stability of composite river banks. *Earth Surface Processes and Landforms*, *6*(5), 469–484. https://doi.org/10.1002/esp.3290060507

U.S. Geological Survey (USGS). (1998). *DOQQ_1998 1998–99 Aerial Photos*. Indiana, produced by the United States Geological Surgery (USGS). Retrieved from https://maps.indiana.edu/arcgis/rest/services/Imagery/DOQQ_1998/MapServer

U.S. Geological Survey (USGS). (2023). National Water Information System data available on the World Wide Web (USGS Water Data for the Nation). Retrieved from https://waterdata.usgs.gov/monitoring-location/03360500/

van de Lageweg, W. I., van Dijk, W. M., Baar, A. W., Rutten, J., & Kleinhans, M. G. (2014). Bank pull or bar push: What drives scroll-bar formation in meandering rivers? *Geology*, *42*(4), 319–322. https://doi.org/10.1130/G35192.1

Weisscher, S. A. H., Shimizu, Y., & Kleinhans, M. G. (2019). Upstream perturbation and floodplain formation effects on chute-cutoff-dominated meandering river pattern and dynamics. *Earth Surface Processes and Landforms*, *44*(11), 2156–2169. https://doi.org/10.1002/esp.4638

Widhalm, M., Hamlet, A., Byun, K., Robeson, S., Baldwin, M., Staten, P., et al. (2018). Indiana's past & future climate: A report from the Indiana Climate Change Impacts Assessment. *Climate Change Reports*. https://doi.org/10.5703/1288284316634

Yamasaki, T. N., Jiang, B., Janzen, J. G., & Nepf, H. M. (2021). Feedback between vegetation, flow, and deposition: A study of artificial vegetation patch development. *Journal of Hydrology*, *598*, 126232. https://doi.org/10.1016/j.jhydrol.2021.126232

Zen, S., Gurnell, A. M., Zolezzi, G., & Surian, N. (2017). Exploring the role of trees in the evolution of meander bends: The Tagliamento River, Italy. *Water Resources Research*, *53*(7), 5943–5962. https://doi.org/10.1002/2017WR020561

Zhao, K., Lanzoni, S., Gong, Z., & Coco, G. (2021). A numerical model of bank collapse and river meandering. *Geophysical Research Letters*, *48*(12), e2021GL093516. https://doi.org/10.1029/2021GL093516